Earth and Planetary Science Letters 304 (2011) 483–495

Contents lists available at ScienceDirect

Earth and Planetary Science Letters

journal homepage: www.elsevier.com/locate/epsl

Structural and geochronological evidence for the leading edge of the Greater Himalayan Crystalline complex in the central Nepal Himalaya

A. Alexander G. Webb [a,*], Axel K. Schmitt [b], Dian He [a], Eric L. Weigand [c,1]

[a] Department of Geology and Geophysics, Louisiana State University, Baton Rouge, LA 70803, USA
[b] Department of Earth and Space Sciences, University of California, Los Angeles, CA 90095, USA
[c] Fugro West, Inc., 4829 McGrath St., Suite 100, Ventura, CA 93003, USA

ARTICLE INFO

Article history:
Received 31 July 2010
Received in revised form 9 February 2011
Accepted 14 February 2011

Editor: R.W. Carlson

Keywords:
South Tibet detachment
Main Central thrust
tectonic wedging
collisional tectonics

ABSTRACT

The Himalaya is commonly described as a three layer-two fault stack. Namely, a high-grade crystalline core featuring an inverted metamorphic field gradient, the Greater Himalayan Crystalline complex (GHC), is separated from units above and below by shear zones. The Lesser Himalayan Sequence (LHS) underlies the GHC below the Main Central thrust, and the Tethyan Himalayan Sequence (THS) overlies it along the South Tibet detachment. However, the southern Main Central thrust hanging wall consists of a lower unit dominated by a right-way-up metamorphic sequence of biotite ± garnet schists (Bhimphedi Group) and an upper unit with only anchizone metamorphism (Pulchauki Group). The Bhimphedi Group is commonly equated to the GHC, while the Pulchauki Group is well correlated to the THS. However, no shear zone separates these units. We present new structural and geochronological data along the boundary between the GHC and the Bhimphedi Group in the Kathmandu region. These data reveal an ~200 m thick Early–Middle Miocene top-north-northeast shear zone that we term the Galchi shear zone. We correlate this shear zone to the South Tibet detachment on the basis of lithological, metamorphic, structural, and chronological criteria. The Galchi shear zone merges with the Main Central thrust to the south, bounding the leading edge of the GHC. This result, combined with recent work in the western Himalaya, suggests that the locally preserved leading edge of the GHC is sub-parallel to the arc of the orogen and the southern Main Central thrust hanging wall is dominated by THS rocks. This orogenic architecture rules out wedge extrusion and channel flow-focused denudation kinematic models for the Himalayan orogen, but is accommodated by tectonic wedging kinematic models, including channel tunneling models with modified timing.

Published by Elsevier B.V.

1. Introduction

Advances in our understanding of the climatic, geochemical, and tectonic aspects of mountain building processes are commonly achieved through study of the Himalayan orogen. The collision of India and Asia is the main cause of contraction and uplift, such that most or all Himalayan rocks were scraped off of the downgoing Indian plate (Argand, 1924; Powell and Conaghan, 1973). Recent work has explored how heterogeneous crustal flow and focused denudation driven by climatic changes may control the kinematic evolution of crystalline rocks in the orogen (e.g., Beaumont et al., 2001; Clift et al., 2008; Grujic et al., 1996, 2006; Hodges et al., 2001; Nelson, 1996; Thiede et al., 2004).

Himalayan geology is described by deformed foreland basin strata along the southern front and three gently north-dipping units stacked by two faults to the north (e.g., Heim and Gansser, 1939; Hodges, 2000). From south to north, these three units are termed: (1) the Lesser Himalayan Sequence (LHS), largely comprised of Proterozoic (meta-)sedimentary rocks; (2) the Greater Himalayan Crystalline complex (GHC), dominated by high grade paragneisses and leucocratic migmatite in a famously inverted metamorphic sequence; and (3) the Tethyan Himalayan Sequence (THS), largely comprised of late Proterozoic to Eocene (meta-)sedimentary rocks (Fig. 1) (e.g., Hodges, 2000; Le Fort, 1975; Yin, 2006). A fourth unit, the Bhimphedi Group, is commonly interpreted as the southern continuation of the GHC despite lacking an inverted metamorphic pattern (e.g., Gehrels et al., 2006a; Upreti and Le Fort, 1999). The GHC overlies the LHS along the top-south Main Central thrust and underlies the THS along the South Tibet detachment (STD) (e.g., Burchfiel and Royden, 1985; Burg et al., 1984; Heim and Gansser, 1939).

The South Tibet detachment is a key factor in current tectonic models because it contains records of alternating top-south and top-north shearing (e.g., Godin et al., 1999; Grujic et al., 2002; Hodges et al., 1996; Jain et al., 1999; Patel et al., 1993; Robinson et al., 2006; Webb et al., 2007). As a gently north-dipping structure with top-north sense-of-shear indicators, the South Tibet detachment has the appearance of a regional low-angle normal fault with extension

* Corresponding author.
E-mail address: awebb@lsu.edu (A.A.G. Webb).
[1] Now at: Fugro Middle East, P.O. Box 2863, Dubai, United Arab Emirates.

0012-821X/$ – see front matter. Published by Elsevier B.V.
doi:10.1016/j.epsl.2011.02.024

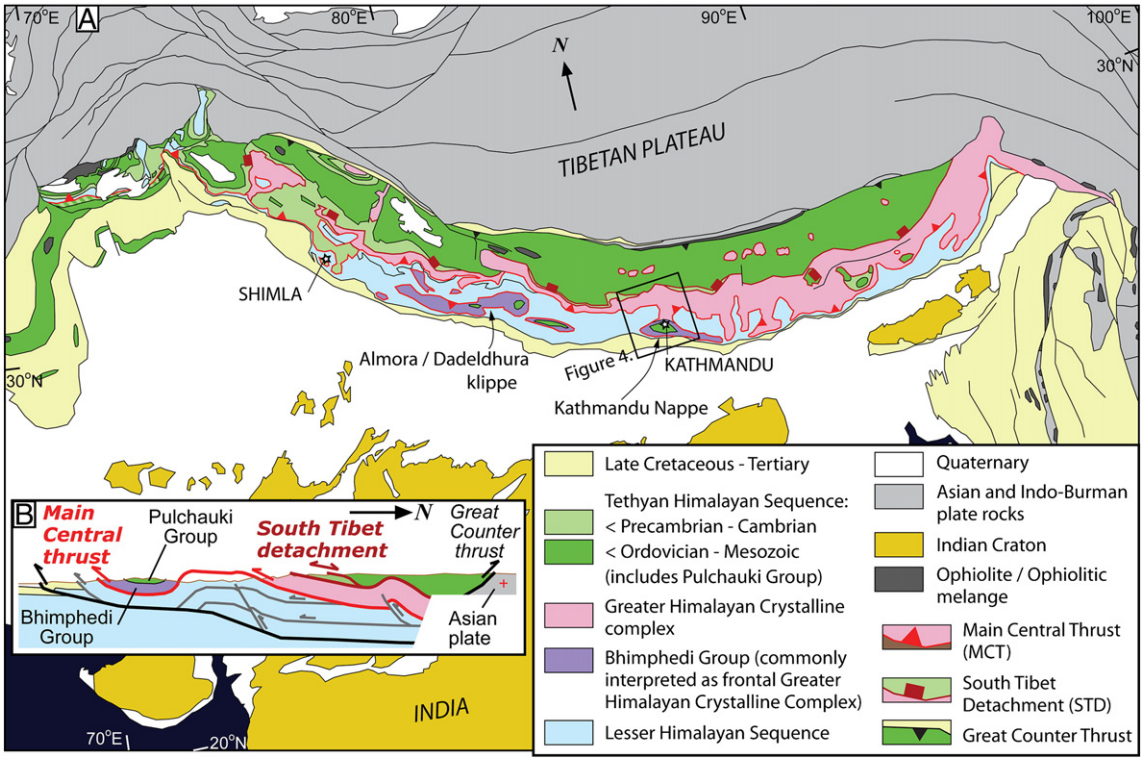

Fig. 1. A. Simplified geological map of the Himalaya, based on Aikman et al. (2008), DiPietro and Pogue (2004), Larson et al. (2010a), Long and McQuarrie (2010), Mitchell et al. (2007), Rao et al. (2000), Webb et al. (2007), Yin and Harrison (2000), Yin (2006), and Yin et al. (2010). B. Schematic cross section across the central Himalaya.

parallel to the shortening direction across the orogen (e.g., Burchfiel et al., 1992; Burg et al., 1984; Herren, 1987).Shortening and extension appear synchronous, as the Main Central thrust and South Tibet detachment were coevally active in the Early–Middle Miocene (e.g., Hodges et al., 1992, 1996).

There are three models explaining the emplacement of the Himalayan crystalline core (the GHC rocks) between the LHS and the THS (Fig. 2): wedge extrusion (e.g., Burchfiel and Royden, 1985; Grujic et al., 1996; Kohn, 2008), channel flow coupled to focused denudation (e.g., Beaumont et al., 2001; Hodges et al., 2001), and tectonic wedging (Webb et al., 2007; Yin, 2006). Wedge extrusion envisions the GHC as a northward-tapering wedge extruding to the south between the two lower grade sequences. The South Tibet detachment kinematics may be driven by rotation of principal stresses along the topographic front that generates upper-crustal extension along the range crest (Burchfiel and Royden, 1985), or may represent adjustments to maintain critical taper if the range is modeled as a Coulomb wedge (e.g., Kohn, 2008; Robinson et al., 2006). In channel flow-focused denudation models, the GHC represents partially molten lower/middle crust in the thickened collision zone that tunnels southwards, driven by the gravitational potential of the high plateau (e.g., Beaumont et al., 2001, 2004; Godin et al., 2006a). This material channel is exhumed between active faults by erosion across a narrow zone where precipitation is focused by the orography of the topographic front (e.g., Beaumont et al., 2001; Hodges et al., 2001). The initiation of rapid exhumation and development of the paired channel flow-focused denudation system is speculated to result from a precipitation increase associated with a climatic shift (e.g., Beaumont et al., 2001; Clift et al., 2008; Hodges et al., 2001). In tectonic wedging models, top-north motion along the South Tibet detachment does not represent extension, but rather 10 s of kilometers of back thrusting in the Main Central thrust hanging wall. The top-north displacement is kinematically linked to the north-directed Great Counter thrust system, which juxtaposes the THS rocks atop the Asian plate rocks and suture zone rocks to the north and was active in the Early–Middle Miocene (i.e., coeval with South Tibet detachment motion; Yin et al., 1994, 1999). This model was motivated by the discovery that the Main Central thrust and South Tibet detachment merge to the south in the western Himalaya, bounding the locally exposed leading edge of the GHC (Thakur, 1998; Webb et al., 2007; Yin, 2006).

In this work we conduct preliminary tests of these models in the central Himalaya. We focused our efforts by noting that in the western Himalaya, the Main Central thrust–South Tibet detachment branch line at the leading edge of the GHC is associated with a north–south transition in the Main Central thrust hanging wall: from kyanite-bearing rocks with an inverted metamorphic pattern in the north to garnet-bearing rocks with a right-way-up metamorphic pattern in the south (Epard et al., 1995; Webb et al., 2007). For this study we examined the same metamorphic transition in the Kathmandu Nappe region, as defined in the work of Rai et al. (1998) and Johnson et al. (2001). Below we review the regional geology, present new structural and geochronological constraints, and integrate these in a kinematic model of the central Himalaya.

2. Geological background

2.1. Orogenic framework

Metamorphic variations across the Himalayan units are important guides for testing Himalayan tectonic models. The GHC forms the crystalline core of the range and displays an inverted metamorphic field gradient with garnet ± staurolite ± kyanite bearing rocks at the base and sillimanite + migmatite bearing rocks at the top (e.g., Catlos et al., 2001; Hubbard, 1996; Jamieson et al., 2004; Kohn, 2008; Le Fort, 1975; Vannay and Grasemann, 1998). Metamorphic grade increases up-section in the LHS and downsection in the THS: structurally high, northerly portions of the LHS and the structurally lowest portions of the THS commonly exhibit amphibolite facies metamorphic rocks (e.g., Beyssac et al., 2004; Bollinger and Janots, 2006; Catlos et al., 2001, 2004; Célérier et al., 2009a,b; Chambers et al., 2009; Gleeson and Godin, 2006; Jain et al., 1999; Jessup et al., 2008; Vannay et al.,

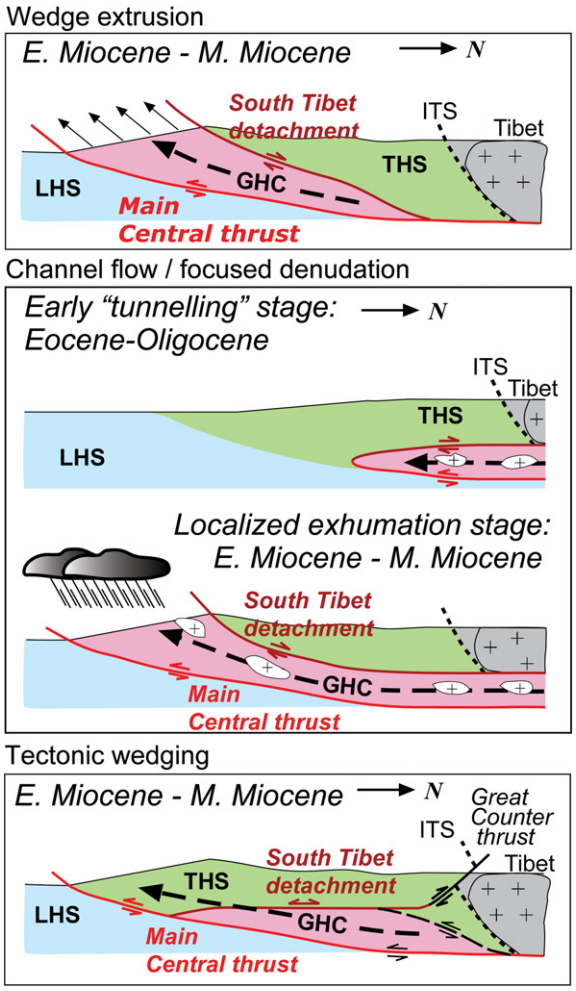

Fig. 2. Himalayan tectonic models, units as in Fig. 1.

1999). Therefore in many localities, metamorphic conditions are continuous and nearly unchanged across GHC boundaries (e.g., Chambers et al., 2009; Gleeson and Godin, 2006; Grujic et al., 2002; Jain et al., 1999; Jessup et al., 2008; Vannay et al., 1999).

The Main Central thrust is a top-south shear zone, active in the Early and Middle Miocene, that has accommodated >100 km of slip (e.g., Catlos et al., 2002; Daniel et al., 2003; DeCelles et al., 2001; Heim and Gansser, 1939; Hodges et al., 1992, 1996; Hubbard and Harrison, 1989; Schelling and Arita, 1991). Strands of the shear zone show an irregular trace extending ~100 km perpendicular to the Himalayan thrust front in many locations along the range (Fig. 1) (e.g., DiPietro and Pogue, 2004; Gansser, 1964; Grujic et al., 2002; Yin, 2006). Northern exposures of the Main Central thrust are locally coincident with a zone of Late Miocene to recent (likely active) top-south thrusting (e.g., Harrison et al., 1997, 1998; Searle et al., 2008; Wobus et al., 2005). Locally this younger shear zone diverges from the trace of the older Main Central thrust and deforms it within south-verging folds of ~5–10 km amplitudes (e.g., Robinson and Pearson, 2006; Thiede et al., 2004, 2005; Valdiya, 1980; Vannay et al., 2004). The younger fault strands, termed the MCT-I or Munsiari thrust, are interpreted by some to represent continued or reactivated motion along the length of the earlier Main Central thrust(e.g., Harrison et al., 1998).We classify only the earlier (Early and Middle Miocene) strands as the Main Central thrust (MCT).

Southerly portions of the Main Central thrust in the central Himalaya are largely exposed at the base of klippen (Fig. 1) (e.g., DeCelles et al., 2001; Johnson, 2005; Johnson et al., 2001; Upreti and Le Fort, 1999). The crystalline rocks here do not display the famous inverted metamorphic sequence associated with the GHC, but instead have a right-way-up metamorphic sequence. Therefore these rocks are commonly classified separately from the GHC and termed the Lesser Himalayan Crystalline Nappes or the Bhimphedi Group (e.g., Upreti and Le Fort, 1999). Rare northerly kyanite ± migmatite gneisses and dominant garnet schists occur at the base, and grade progressively decreases upsection, past the biotite-in isograd, up to weakly metamorphosed Early Paleozoic rocks of the THS (e.g., Gehrels et al., 2006a,b; Rai et al., 1998; Stöcklin, 1980; Upreti and Le Fort, 1999; Valdiya, 1980). These THS rocks are termed the Pulchauki Group (e.g., Upreti and Le Fort, 1999). Although elsewhere in the Himalaya THS rocks commonly occur in the South Tibet detachment hanging wall, here no large shear zone is reported between the Main Central thrust and the Pulchauki Group (e.g., Gehrels et al., 2003, 2006a; Johnson et al., 2001).

Two fault strands are increasingly recognized along parts of the South Tibet detachment, with structurally lower ductile strands commonly succeeded by structurally higher, and lower temperature strands (e.g., Hodges et al., 1996; Cottle et al., 2007). Amphibolite grade metamorphic rocks that commonly occur between the two strands are variably interpreted as Greater Himalayan Crystalline complex or Tethyan rocks (e.g., cf. Godin et al., 2006b and Kellett et al., 2009). The lowermost South Tibet detachment fault parallels and closely coincides with the right-way-up kyanite isograd and/or the right-way-up peak metamorphic temperature decrease from ~700–650 °C to ~650–500 °C along the orogen (Brown and Nazarchuk, 1993; Burchfiel et al., 1992; Cottle et al., 2007; Dèzes et al., 1999; Godin et al., 2001; Grujic et al., 2002; Herren, 1987; Hodges et al., 1996; Jessup et al., 2008; Metcalfe, 1993; Patel et al., 1993; Searle, 1986; Valdiya, 1989; Vannay and Grasemann, 1998). Where Tethyan and Greater Himalayan rocks are separated by a single South Tibet detachment fault zone, such as in the Shimla region, basal Tethyan rocks commonly record temperatures of >600 °C (Fig. 1, e.g., Chambers et al., 2009).

The Bhimphedi Group of the southern Main Central thrust hanging wall is not considered by Himalayan tectonic models (cf. Figs. 1 and 2) as most authors classify the sekyanite and garnet bearing rocks as frontal portions of the GHC (e.g., Arita et al., 1997; Bollinger et al., 2006; Gehrels et al., 2006a; Johnson et al., 2001; Robinson et al., 2003). Three potential scenarios are commonly suggested (Fig. 3A–C): (A) a South Tibet detachment contact does occur between the Bhimphedi Group and the Pulchauki Group, but has yet to be identified because of poor exposure (e.g., Yin, 2006). (B) The Pulchauki Group was deposited on the southerly GHC rocks, and the whole package occurs south of the position where the South Tibet detachment breached the surface (e.g., Gehrels et al., 2003; Johnson, 2005). (C) The Bhimphedi and Pulchauki groups are restricted to the footwall of the Main Central thrust (e.g., Hodges, 2000; Rai et al., 1998; Upreti and Le Fort, 1999). The fault at the base of the Bhimphedi Group is not interpreted as the Main Central thrust, but rather as a relatively minor synchronous thrust deforming the LHS (the term Mahabarat thrust is used to signify this proposed distinction). The Bhimphedi Group rocks are likewise re-interpreted as LHS rocks. The Pulchauki Group rocks are interpreted to represent the southernmost extent of the Tethyan basin, deposited south of the Cenozoic Main Central thrust. These interpretations are generally compatible with models for GHC emplacement, although cross-section A requires the GHC to taper to the south, contrary to predictions of wedge extrusion models, and cross-section B requires the GHC to taper to the north, contrary to predictions of tectonic wedging models.

However, a fourth type of solution for the Bhimphedi Group question could have important impacts on the range of possible Himalayan kinematic models. It would involve a southerly merger of the Main Central thrust and South Tibet detachment, as seen in the western Himalaya (Fig. 3D). Both the Pulchauki Group and the Bhimphedi Group would consist of THS rocks to the south of the branch line of the two

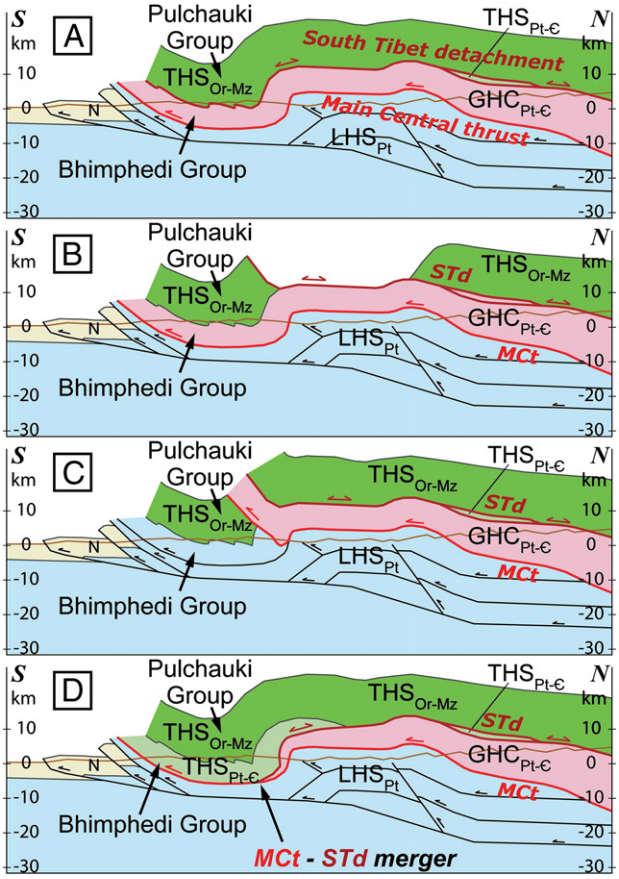

Fig. 3. Cross-sections with differing interpretations of the Bhimphedi Group, units as in Fig. 1. References as discussed in text, except: the Lesser Himalayan duplex modified from Bollinger et al. (2004), Pearson and DeCelles (2005), and Wobus et al. (2005).

faults, with the northerly kyanite + migmatite gneiss representing the leading edge of the GHC. Since the GHC leading edge would be locally buried at locations like the northern margins of the Kathmandu Nappe and Dadeldhuraklippe, it would remove wedge extrusion models and severely limit the role that focused denudation could play in exhuming the frontal tip of a GHC channel in the Early and Middle Miocene. Miocene deposits of Late Proterozoic detritus interpreted to reflect GHC exhumation could instead reflect other Late Proterozoic sequences such as the Bhimphedi Group (Yin, 2006).

The thermal profile of the proposed THS-dominated Bhimphedi–Pulchauki succession would match the hot-base (~600 °C), right-way-up thermal signatures that are increasingly recognized in the immediate South Tibet detachment hanging wall (e.g., Chambers et al., 2009; Gleeson and Godin, 2006; Jessup et al., 2008; Vannay et al., 1999). The Shimla region offers an analog to this proposed scenario, as the South Tibet detachment and Main Central thrust merge in the up-dip direction here (Fig. 1; Thakur, 1998; Webb et al., 2007; Yin, 2006). The Main Central thrust hanging wall to the south of this merger is lithologically, structurally, and thermobarometrically continuous with the THS rocks of the South Tibet detachment hanging wall (Webb et al., 2007; see also Thakur, 1998; Yin, 2006). THS rocks at the base of the southern Main Central thrust hanging wall record high peak temperatures (~550–650 °C), similar to both the base of the South Tibet detachment hanging wall and to the base of the GHC along the northern Main Central thrust (Epard et al., 1995). However, the metamorphic field gradient is right-way-up, decreasing to biotite grade at ~4 km structurally above the southern Main Central thrust (Epard et al., 1995).

The ideal site to test these differing concepts for the structural evolution of the central Himalayan Main Central thrust hanging wall would be an area that involves continuous exposure of the Main Central thrust from the northern hinterland, where it underlies GHC rocks, to the south where it underlies the Bhimphedi Group. The Kathmandu region offers such an opportunity (Figs. 1 and 4). Below, we review existing knowledge of the Kathmandu region.

2.2. Regional geology

The Main Central thrust hanging wall in the Kathmandu region varies from GHC rocks in the north, to correlative rocks termed the Sheopuri Gneiss (dominantly ± kyanite ± sillimanite ± migmatite paragneiss), to a Bhimphedi–Pulchauki succession which dominates the synformal Kathmandu Nappe (e.g., Gehrels et al., 2006a; Johnson et al., 2001; Kohn et al., 2001; 2004; Rai et al., 1998; Stöcklin and Bhattarai, 1982). The Bhimphedi Group is an ~5 km thick package of Late Proterozoic meta-sedimentary rocks intruded by Cambro-Ordovician granites. The overlying anchizone/unmetamorphosed rocks of the Ordovician–Devonian Phulchauki Group are correlative to THS rocks of the same age to the north (Gehrels et al., 2006a; Johnson et al., 2001). The Main Central thrust at the base of the Kathmandu Nappe is also termed the Mahabharat thrust, and it consists of a ~1 km thick ductile shear zone (e.g., Johnson et al., 2001; Stöcklin, 1980). The boundary between the Bhimphedi Group and the GHC-correlative Sheopuri Gneiss is not well understood, but it is known to be roughly coincident with the right-way-up kyanite-isograd. This contact intersects the Main Central/Mahabharat thrust plane along the northern margin of the Kathmandu Nappe (Johnson et al., 2001; Rai et al., 1998; Stöcklin, 1980). The contact also marks the approximate border between the high grade inverted metamorphic sequence and the right-way-up metamorphic gradient observed across the Kathmandu Nappe (Johnson et al., 2001). The right-way-up gradient is quantified by Johnson et al. (2001), who use thermobarometric analysis and regional isograd mapping to illustrate a decrease in the peak metamorphic temperatures from 675-600 °C in the southernmost Sheopuri/GHC rocks, through ~500 °C in Bhimphedi Group garnet schists, to anchizone conditions in the structurally highest Phulchauki Group.

Because the Bhimphedi Group is commonly correlated with the GHC, and the overlying Phulchauki Group is well correlated to THS rocks, the South Tibet detachment is speculated to occur either along the contact of these two units or within upper stratigraphic levels of the Bhimphedi Group (Yin, 2006). South-directed thrusts occur within the Kathmandu Nappe, but no significant shear zone with top-north shear has been identified, and contacts between major formations appear depositional (Gehrels et al., 2003; 2006a). The only reports of top-north shearing in the Kathmandu area are (1) shear bands in the southern Sheopuri rocks (Rai et al., 1998) and (2) a photo of leucogranite cut by apparently top-north asymmetric boudinage in the westernmost Sheopuri–Bhimphedi contact zone (the region of the Fig. 5 map, as indicated in Fig. 4; the photo is Fig. 5b from Johnson et al., 2001). Johnson et al. (2001) acquired TIMS U–Pb zircon data for the leucogranite; these data define a discordant trend extending from the Early Paleozoic to $18.3 + 1.9/-2.2$ Ma.

Additional geochronological constraints on the timing of Kathmandu Nappe deformation include Early Paleozoic U–Pb zircon ages of granites cross-cutting south-directed thrusts in the Bhimphedi and Phulchauki groups, Early Paleozoic and Late Oligocene Th–Pb dates on monazites included in Bhimphedi Group garnets, and $^{40}Ar/^{39}$ muscovite ages from both the footwall and hanging wall of the Main Central thrust which smoothly decrease in age from ~20 Ma at the southern margin of the Kathmandu Nappe to ~14 Ma at the northern margin (Arita et al., 1997; Bollinger et al., 2004; Gehrels et al., 2003, 2006a; Herman et al., 2010). The zircon ages demonstrate that at least some south-directed thrusting observed within the Bhimphedi and Phulchauki groups occurred in the Early Paleozoic. The Th–Pb data record Early Paleozoic and Late Oligocene prograde metamorphism in the Bhimphedi Group. The muscovite ages reveal

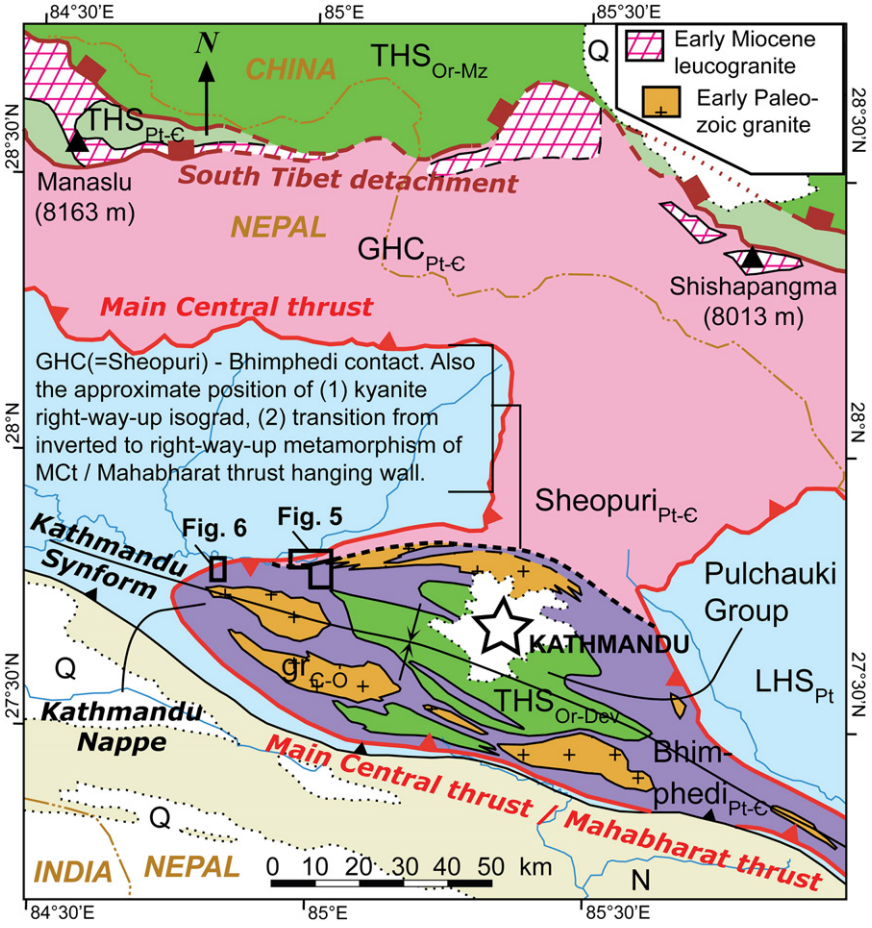

Fig. 4. Geological map of the Kathmandu region, units as in Fig. 1 except as specified. Modified from: Burchfiel et al. (1992), Gehrels et al. (2006a), Godin et al. (2006b), Johnson et al. (2001), Searle and Godin (2003), Searle et al. (1997), Stöcklin(1980), Stöcklin and Bhattarai(1982), and our mapping.

progressive cooling of the Kathmandu Nappe from south to north, requiring cessation of ductile deformation in the Early Miocene to the south, and in the Middle Miocene to the north.

3. Structural geology

In order to better understand the nature of the southern Main Central thrust hanging wall and the transition from GHC/Sheopuri rocks in the north to the Bhimphedi Group in the south, we conducted field mapping of two (north–south) transects across the northern margin of the Kathmandu Nappe(Figs. 4–6). The transects are along the Mahesh Khola (khola = river), ~50 km west-northwest of Kathmandu, and along the Malekhu Khola, ~25 km farther west (Figs. 4–6). Previous mapping and analytical work along these sections by Johnson et al. (2001) and Pearson and DeCelles (2005) established the lithologic distribution, metamorphic field gradients, positions of the Ramgarh thrust and the Main Central thrust shear zone, and the contact between Early Proterozoic (LHS) and Late Proterozoic (GHC/Bhimphedi Group) rocks within the Main Central thrust zone (via detrital zircon and Nd isotopic analysis).

3.1. Mahesh Khola

This transect extends across the LHS, GHC/Sheopuri, and Bhimphedi Group rocks which dip steeply to the south-southeast within the northern limb of the Kathmandu Synform, such that structural elevation increases to the south (Figs. 4 and 5).The Main Central thrust here is an ~1100 m thick shear zone dominated by S–C fabric (Fig. S1). Sense of shear within the steeply dipping shear zone is oblique and right-lateral, with the southern block moving down along a line plunging moderately to the west-southwest. By rotating the S–C fabric to a sub-horizontal syn-deformation orientation (the non-cylindrical shape of the Kathmandu Synform adds complexity to this task, see Fig. S2) we interpret a top-south-southwest sense of shear. Rocks in the Main Central thrust shear zone are garnet phyllonites within the northern Early Proterozoic LHS portion and garnet mica schists within the southern Late Proterozoic rocks. The metamorphic field gradient is inverted across the Main Central thrust and its immediate footwall, progressing across the garnet-in and kyanite-in isograds.

The immediate Main Central thrust hanging wall contains an ~300 m thick section of quartz-rich garnet mica schists. These rocks are differentiated from the Main Central thrust because the dominant structural fabric is mica foliation, with S–C fabric occurring in only an ~10 m thick layer (this layer occurs in the middle of the section and has consistent shear sense with the Main Central thrust). At the top of this section, the schistose fabric is replaced by gneissic banding across an ~20 m thick transition into garnet-tourmaline-mica gneiss.

The overlying gneiss section is ~200 m thick, consists of psammitic and pelitic rocks with minor leucogranitic lenses, and is strongly deformed, forming a shear zone that we term the Galchi shear zone after a local village. The Galchi shear zone features diverse structural fabrics (Fig. 7, Fig. S1). Early structures include sheath folds, which fold early gneissic foliation. The sheath folds dominate the basal ~30 m of the shear zone, and occur across its entire thickness. The main foliation contains mineral stretching lineations defined by biotite, feldspar, and tourmaline which are parallel to the long axes of the sheath folds, plunging moderately to the west-southwest (see Fig. 5, Galchi shear zone stereo net). S–C fabric, S–C′ fabric, sigma-type

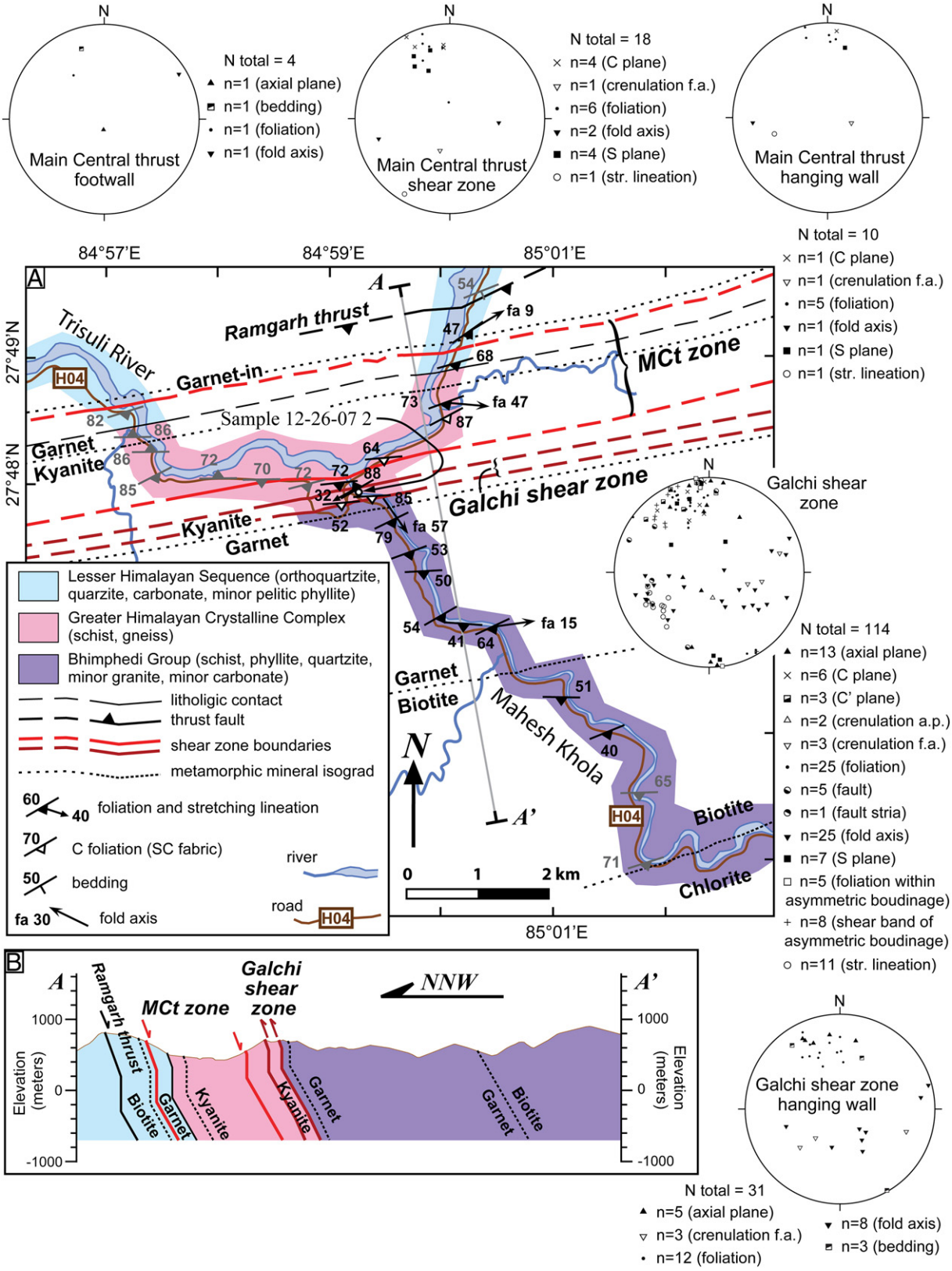

Fig. 5. A. Geological map of the Mahesh Khola transect, with equal area stereo plots of structural data. After Johnson et al. (2001), Pearson and DeCelles (2005), and our own observations; map data in gray are from Johnson et al. (2001) and Pearson and DeCelles (2005). B. Cross-section A–A′.

porphyroclasts, and meter-scale asymmetric boudinage occur across the shear zone and are also congruent with the lineations. Leucogranitic lenses are foliated and deformed by asymmetric boudinage, indicating that they are pre- and/or syn-kinematic. Sparse late structures include decimeter-scale bookshelf normal fault systems and meter-scale thrust faults with associated cylindrical folds. Excepting decimeter-scale antithetic thrust faults, all structures have a consistent sense of shear: the Galchi shear zone appears to be

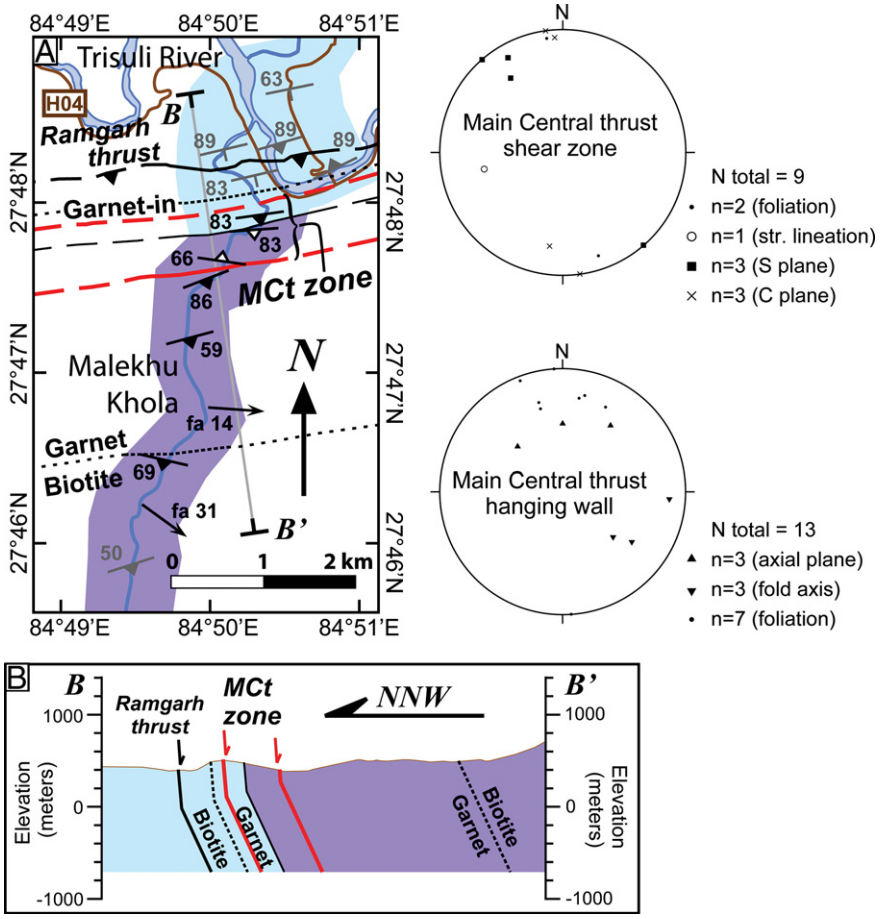

Fig. 6. A. Geological map of the Malekhu Khola transect, with equal area stereo plots of structural data. For legend, see Fig. 5A. After Johnson et al. (2001), Pearson and DeCelles (2005), and our own observations; map data in gray are from Johnson et al. (2001) and Pearson and DeCelles (2005). B. Cross-section A–A′.

an east-northeast striking steep oblique fault with left-lateral, south-block-up motion. Therefore the Galchi shear zone is parallel to the Main Central thrust and has an opposite shear sense. Rotation of the Galchi shear zone structures to remove Kathmandu Synform folding (see Fig. S2) yields a sub-horizontal shear zone with a top-north-northeast sense of shear.

Rocks south of the Galchi shear zone are dominantly micaceous quartzites, garnet-biotite schist, and biotite schist. An ~100 m thick foliated granite sill occurs ~3 km south of the Galchi shear zone. Detailed petrologic and thermobarometric investigations by Johnson et al. (2001) position the kyanite isograd ~150 m south of the Galchi shear zone within a right-way-up metamorphic field gradient. Quartzite dominates the ~100 m thick section immediately above the Galchi shear zone and contains meter-scale tight asymmetric cylindrical folds of parallel bedding and micaceous foliation. The fold asymmetry suggests an oblique left-lateral shear sense in present orientation, consistent with Galchi shear zone motion. Farther south through the garnet isograd, we observe meter scale tight folds of preserved bedding with shallow east-northeast plunging fold axes and steeply south-southeast dipping axial planes. Foliation in micaceous schists is locally folded within fold noses, but dominantly oriented with the axial planes of the folds; bedding is preserved in quartz-rich rocks.

The schists and gneisses within and to the north of the Galchi shear zone are consistent with previous descriptions of the GHC/Sheopuri gneiss (e.g., Rai et al., 1998; Stöcklin, 1980). Rocks south of the Galchi shear zone match prior descriptions of the Bhimphedi Group and are not offset by large-scale structures across the core of the Kathmandu Synform, consistent with the structural position of the Bhimphedi Group (e.g., Gehrels et al., 2006a,b; Stöcklin, 1980). We therefore interpret the Galchi shear zone as the structural boundary between the GHC/Sheopuri gneiss and the Bhimphedi Group.

3.2. Malekhu Khola

Approached from the north or south, the Malekhu Khola geology appears to match observations along the Mahesh Khola. The transect extends across a similar part of the Kathmandu Synform, with rocks and structures again dipping steeply to the south-southeast and structural elevation increasing to the south (Fig. 6). However, the Galchi shear zone gneiss and fabrics and the underlying foliated quartz-rich garnet mica schists are absent.

The Main Central thrust here is an ~600 m thick shear zone dominated by S–C fabric; quartzite and phyllonite of the LHS portion of the Main Central thrust also features asymmetric boudinage and tension gashes (Fig. S1). The southern Late Proterozoic portion of the Main Central thrust zone is dominated by garnet mica schist. Sense of motion in present orientation is right-lateral and oblique with the south-block moving down. A <100 m thick layer of marble occurs immediately above the Main Central thrust zone. To the south of this layer micaceous quartzites, garnet-biotite schist, and biotite schist dominate; an ~200 m thick foliated granitic sill occurs ~1.5 km south of the marble. Metamorphic grade is inverted across the Main Central thrust but right-way-up in its hanging wall: no gneiss or leucogranitic rocks are observed, and the garnet isograd occurs ~2 km above the shear zone. Bedding and (commonly coincident) foliation are folded, and locally refolded, in tight to open cylindrical folds south of the Main Central thrust. The folds are dominantly asymmetric with oblique top-south-southwest vergence, consistent with the Main

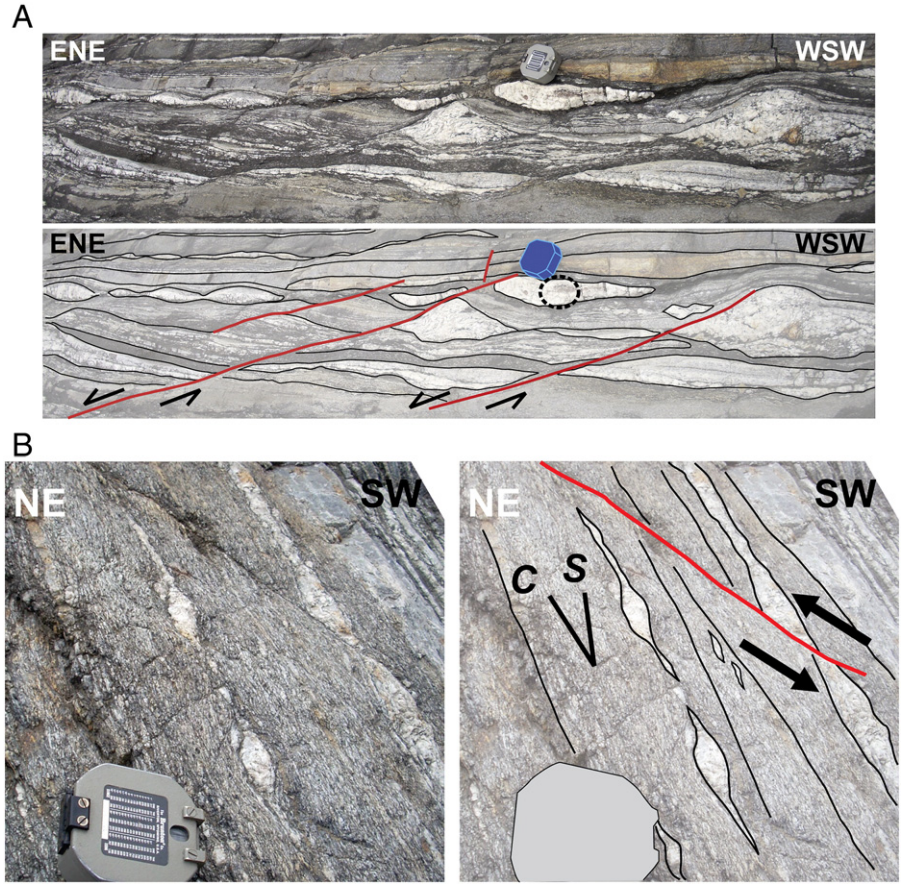

Fig. 7. Field photographs of deformation fabrics in the Galchi shear zone (Mahesh Khola transect). A. Composite photograph and line diagram of top-northeast asymmetric boudinage showing shear bands off-setting gneissic foliation and leucogranitic lenses. Site is ~30 m structurally above the base of the shear zone along Mahesh Khola (Fig. 5). Dashed oval indicates dated leucogranite sample 12-26-07 2 (see Geochronology, Fig. 8). Brunton compass for scale, view looking towards east-southeast and down ~50°. B. Photograph and line diagram of top-northeast shear band and sigma-type porphyroclasts. Site is ~80 m above the base of the shear zone along Mahesh Khola. Brunton compass for scale, view looking towards southeast and down ~40°.

Central thrust at the base (Fig. S1). The lithologies, right-way-up metamorphic field gradient, and structural continuity observed across the Main Central thrust hanging wall here are consistent with the Bhimphedi Group.

4. Geochronology

We obtained crystallization ages on zircons from a leucogranitic lens deformed by top-north shear within the Galchi shear zone (sample 12-26-07 2, shown in Fig. 8A) to constrain the timing of top-north motion. 36 U–(Th)–Pb spot data from 24 zircon grains were acquired using the CAMECA *ims* 1270 ion microprobe at UCLA with procedures reported in Schmitt et al. (2003). This work was accomplished using an 8–15 nA O^- primary beam focused to an ~15 μm diameter spot which generated a crater depth of ~1 μm during the analysis duration. U–Pb ratios were determined using a calibration curve based on UO/U vs. Pb/U analyzed on zircon standard AS3 (age 1099.1 Ma, Paces and Miller, 1993), and radiogenic isotopic ratios were calculated using common Pb ratios for the Late Cenozoic (Stacey and Kramers, 1975). During each of the two analytical sessions U/Zr and Th/Zr relative sensitivities were determined on zircon standard 91500 (U and Th concentrations are 81.2 and 28.6 ppm, respectively, Wiedenbeck et al., 1995) to estimate U and Th abundances of the unknowns. Data reduction was accomplished via the in-house program ZIPS 3.0 (developed by Chris Coath).

Cathodoluminescence imagery of the grains reveals complex grain cores with thin (≤35 μm) prismatic rims (Fig. 8A). 10 spot analyses targeted grain cores. The remaining 26 spot analyses targeted grain rims, but because the rims are thin, these analyses commonly overlap the grain interiors. Spot data from grain cores have variable, Paleozoic to Eocene $^{238}U/^{206}Pb$ ages and low U/Th (~50 to 170) (Table 1, Fig. 8). Spot data targeting grain rims have Paleozoic to Early Miocene $^{238}U/^{206}Pb$ ages. Of these, the youngest age is ~20 Ma, and the youngest age cluster (seven ages) spans from ~24 to 30 Ma. U/Th is commonly low for the rim-targeting analyses, but shows an increasing spread towards elevated ratios with younger ages. For rim analyses with $^{238}U/^{206}Pb$ ages less than 30 Ma, U/Th ranges from ~50 to ≥2000.

We interpret this range of zircon ages to represent mixing between inherited interior and neoblastic rim domains. The youngest ages likely represent the crystallization of the leucogranite at ~24 to 30 Ma, or perhaps as young as ~20 Ma. This interpretation is bolstered by high U/Th in many young analyses, because high U/Th commonly denotes zircon that grew in equilibrium with metamorphic fluids and during anatexis (e.g., Hoskin and Black, 2000; Rubatto, 2002; Rubatto et al., 2006).The 30–20 Ma ages therefore provide an upper age limit on the top-north shearing that deforms the leucogranite.

5. Discussion

Our mapping documents the presence of an ~200 m thick top-north-northeast shear zone, termed the Galchi shear zone, along the northern margin of the Kathmandu Nappe. The Galchi shear zone juxtaposes the GHC with the Bhimphedi Group and spatially correlates to the right-way-up kyanite isograd. The kyanite isograd intersects the Main Central thrust to the west, i.e., towards the foreland along the fault (Johnson et al., 2001). The Galchi shear zone

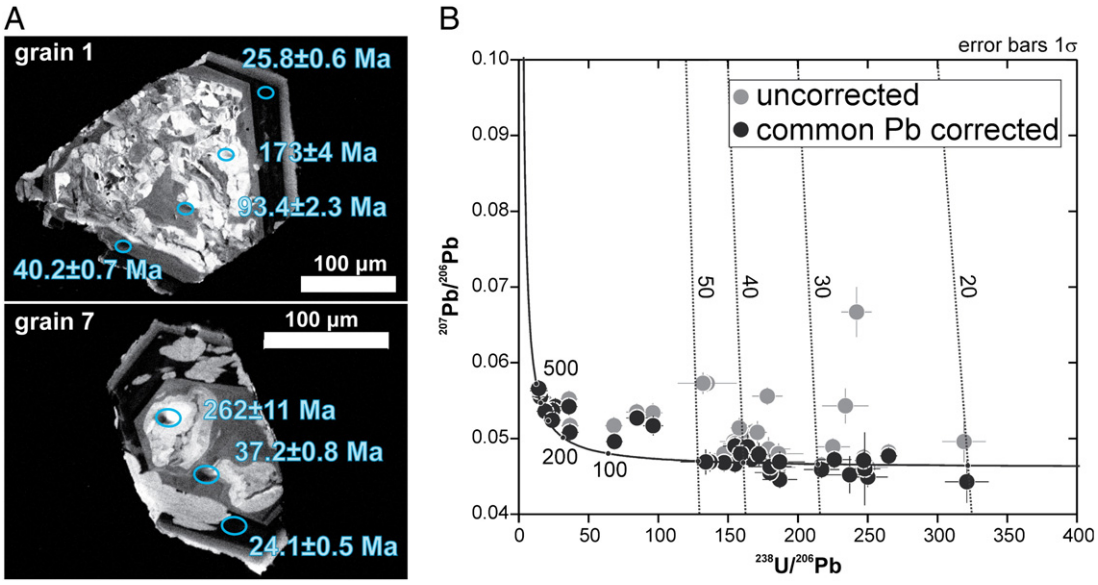

Fig. 8. U–(Th)–Pb zircon geochronology of sample 12-26-07 2. A. Cathodoluminesence images of selected zircon grains and $^{238}U/^{206}Pb$ spot ages. B. $^{207}Pb/^{206}Pb$ vs. $^{238}U/^{206}Pb$ concordia diagram showing data prior and after common-Pb correction. Numbers indicate age in Ma, with mixing trajectories between radiogenic and common-Pb (~0.828; Schmitt et al., 2003) indicated.

likewise does not appear along a transect west of this intersection line. Ductile shearing along the Galchi shear zone occurred between ~20–30 Ma and ~14 Ma, as constrained by our ages of a deformed leucogranite and published $^{40}Ar/^{39}$ muscovite thermochronology, respectively (see above, or summary in Bollinger et al., 2004). Below we discuss the implications of these findings for the kinematic evolution of the Himalayan orogen.

5.1. The Galchi shear zone and the leading edge of the GHC

As a top-north shear zone bounding the top of the GHC, the Galchi shear zone may represent the southern extension of the South Tibet detachment. This interpretation is consistent with the following criteria: lithological juxtaposition, metamorphic correlations, structural fabrics, and timing of deformation. Lithologies on both sides of the lowermost South Tibet detachment in most other parts of the Himalaya include Late Proterozoic metasedimentary rocks, mid-Cenozoic leucogranites, and Early Paleozoic granites (e.g., Burchfiel et al., 1992; Godin et al., 2006b; Grujic et al., 2002; Hodges et al., 1996; Vannay et al., 2004).Our work, combined with the studies of Johnson et al. (2001) and Gehrels et al. (2003, 2006a), show that Late Proterozoic metasedimentary rocks occur across the Galchi shear zone, mid-Cenozoic leucogranites occur below and within it, and Early Paleozoic granites occur structurally above it. The metamorphic pattern associated with the lowermost South Tibet detachment across the range is remarkably consistent: the shear zone parallels and closely coincides with the right-way-up kyanite isograd and/or the right-way-up peak metamorphic temperature decrease from ~700–650 °C to ~650–500 °C (e.g., Dèzes et al., 1999; Godin et al., 2001; Grujic et al., 2002; Jessup et al., 2008; Vannay and Grasemann, 1998). Likewise, the Galchi shear zone is nearly coincident with this isograd. The right-way-up metamorphic field gradient of the southerly hanging wall of the Galchi shear zone matches the metamorphic pattern observed across the hanging wall of the lowermost South Tibet detachment (e.g., Chambers et al., 2009; Cottle et al., 2007). The structural fabrics of the South Tibet detachment and the Galchi shear zone are a clear match as the only ≥200 m thick shear zones to feature high top-north shear strain within the Himalaya. The immediate hanging wall and footwall of the South Tibet detachment feature pervasive fabric development, with the exception of Early Paleozoic granites of the hanging wall, which are locally undeformed (e.g., Vannay et al., 2004). The Early Paleozoic granites within the Bhimphedi Group of the Galchi shear zone hanging wall are likewise locally undeformed. Finally, ductile shearing within both the South Tibet detachment shear zone and the Galchi shear zone occurred during the Early and Middle Miocene (e.g., see summary in Godin et al., 2006a).

The regional extent of the Galchi shear zone is unclear. It did not occur along our western transect (Malekhu Khola). West of Mahesh Khola, the shear zone likely maintains its close correspondence to the kyanite isograd, suggesting that the Galchi shear zone also intersects the Main Central thrust (Fig. 4). To the east, Rai et al. (1998) report top-north shear bands in the southern Sheopuri gneisses which may relate to the shear zone, particularly if the Galchi shear zone–South Tibet detachment correlation is correct, because diffuse top-north shearing extending kilometers above and below the main shear zone is locally associated with the South Tibet detachment (e.g., Long and McQuarrie, 2010; Patel et al., 1993). We speculate that the Galchi shear zone persists along the contact of the GHC/Sheopuri gneiss and the Bhimphedi Group, and intersects the Main Central thrust on the northeast margin of the Kathmandu Nappe.

The interpretation that the South Tibet detachment occurs along the GHC–Bhimphedi Group transition in the Kathmandu region suggests that both the Bhimphedi Group and the Phulchauki Group represent THS rocks. We therefore favor the cross-sectional interpretation of the Kathmandu Nappe illustrated in Fig. 3D, involving the southwards merger of the Main Central thrust and the South Tibet detachment. We suggest that this interpretation may apply across the entire southern Himalaya, and present a modified Himalayan tectonic map consistent with this interpretation (Fig. 9). This map shows the leading edge of the GHC locally exposed in multiple locations across the Himalaya: the western Himalaya (Thakur, 1998; Webb et al., 2007; Yin, 2006), the northeastern margin of the Almora/Dadeldhuraklippe (based on reinterpretation of lithological and metamorphic data presented by Hayashi et al., 1984), and the Kathmandu Nappe (this work). Farther east, the Main Central thrust–South Tibet detachment intersection line at the frontal tip of the GHC may be entirely eroded away to the south of the South Tibet detachment klippen of Bhutan (e.g., Grujic et al., 2002). Therefore eastwards along the orogen, the intersection line appears increasingly farther south.

A southerly termination of the South Tibet detachment has recently been proposed in Bhutan by Long and McQuarrie (2010).

Table 1
Ion microprobe U–(Th)–Pb zircon data for sample 12-16-07 2.

Spot ID grain #, spot #	$^{206}Pb^*/^{238}U$	±1 s.e.	$^{207}Pb^*/^{235}U$	±1 s.e.	$^{207}Pb^*/^{206}Pb^*$	±1 s.e.	$^{206}Pb^*$ (%)	$^{207}Pb^*$ (%)	Correlation of concordia ellipses	UO/U	U/Th	U (ppm)	Th (ppm)	Ages (Ma) ± 1 s.e.			
														$^{204}Pb/^{206}Pb \times 10^{-3}$	$^{206}Pb^*/^{238}U$	$^{207}Pb^*/^{235}U$	$^{207}Pb^*/^{206}Pb^*$
1, 1	0.00402	0.00010	0.0261	0.0007	0.0471	0.0008	99.9	99.1	0.80	7.94	2003	10,480	5.1	0.0483	**25.8 ± 0.6**	26.2 ± 0.7	54.3 ± 40.0
1, 2c	0.0272	0.0007	0.191	0.005	0.0509	0.0010	99.9	98.3	0.64	7.61	122	679	5.4	0.0643	173 ± 4	177 ± 4	235 ± 48
1, 3c	0.0146	0.0004	0.0999	0.0033	0.0496	0.0011	99.7	95.7	0.75	7.54	154	970	6.2	0.181	93.4 ± 2.3	96.7 ± 3.0	178 ± 50
1, 4	0.00625	0.00011	0.0414	0.0014	0.0480	0.0014	99.6	93.0	0.49	7.81	318	970	3.0	0.402	40.2 ± 0.7	41.2 ± 1.4	101 ± 70
2, 1c	0.0382	0.0010	0.286	0.009	0.0543	0.0005	100.0	100.0	0.97	7.65	104	2200	21	0.0225	242 ± 6	255 ± 7	382 ± 20
2, 2c	0.0445	0.0007	0.326	0.005	0.0532	0.0005	100.0	99.4	0.83	7.80	100	1670	16	0.0318	281 ± 4	287 ± 4	337 ± 20
2, 3c	0.0705	0.0031	0.548	0.023	0.0564	0.0002	100.0	100.0	1.00	7.60	112	3320	29	0.0170	439 ± 18	444 ± 15	468 ± 10
2, 4	0.0413	0.0008	0.306	0.007	0.0538	0.0005	100.0	99.7	0.89	7.59	103	1620	15	0.0382	261 ± 5	271 ± 5	361 ± 23
3, 1	0.0118	0.0010	0.0857	0.0085	0.0528	0.0011	99.9	98.7	0.98	7.65	83.7	2100	24	0.192	75.4 ± 6.7	83.5 ± 8.0	321 ± 47
4, 1c	0.0699	0.0023	0.547	0.018	0.0567	0.0005	100.0	101.0	0.97	7.68	68.0	2990	43	0.0237	436 ± 14	443 ± 12	481 ± 19
5, 1c	0.0277	0.0014	0.207	0.012	0.0543	0.0010	99.9	98.3	0.96	7.66	165	1080	6.4	0.0807	176 ± 9	191 ± 10	383 ± 40
6, 1c	0.0528	0.0010	0.391	0.010	0.0537	0.0005	99.9	97.9	0.95	7.81	81.3	2280	27	0.0166	332 ± 6	335 ± 7	360 ± 23
7, 1	0.00374	0.00007	0.0246	0.0007	0.0477	0.0007	99.9	98.8	0.86	8.23	2131	5700	2.6	0.0768	**24.1 ± 0.5**	24.7 ± 0.7	83.5 ± 37.2
7, 2c	0.00579	0.00013	0.0383	0.0014	0.0480	0.0015	99.6	94.1	0.53	7.74	149	1440	9.4	0.502	37.2 ± 0.8	38.2 ± 1.4	98.0 ± 75.1
7, 3c	0.0415	0.0017	0.300	0.013	0.0524	0.0007	99.9	98.1	0.96	7.54	160	751	4.6	0.0167	262 ± 11	267 ± 10	304 ± 28
8, 1	0.00402	0.00017	0.0255	0.0031	0.0460	0.0048	97.4	67.1	0.52	8.44	98.7	1220	12	1.91	**25.9 ± 1.1**	25.6 ± 3.0	Negative
12, 1	0.0686	0.0055	0.532	0.043	0.0563	0.0002	100.0	99.9	1.00	7.52	106	3640	33	0.0128	428 ± 33	433 ± 28	463 ± 10
16, 1	0.00443	0.00023	0.0288	0.0017	0.0472	0.0008	99.8	96.2	0.95	8.05	57.1	5940	101	0.236	**28.5 ± 1.5**	28.9 ± 1.6	56.8 ± 41.8
17, 1	0.0648	0.0053	0.496	0.040	0.0555	0.0003	99.9	99.2	1.00	7.53	110	2950	26	0.0279	405 ± 32	409 ± 27	433 ± 14
17, 2	0.00537	0.00034	0.0330	0.0022	0.0446	0.0010	99.8	96.2	0.94	7.76	84.4	2540	29	0.546	34.5 ± 2.2	33.0 ± 2.2	Negative
24, 1	0.00462	0.00026	0.0292	0.0017	0.0459	0.0008	99.9	98.6	0.95	8.11	60.8	2710	43	0.0372	**29.7 ± 1.7**	29.2 ± 1.7	Negative
26, 1	0.00646	0.00041	0.0415	0.0027	0.0466	0.0010	99.6	93.6	0.94	7.84	90.1	2230	24	0.540	41.5 ± 2.6	41.3 ± 2.6	29.6 ± 53.2
28, 1	0.00647	0.00035	0.0436	0.0027	0.0489	0.0010	100.0	99.2	0.95	8.20	84.9	2240	26	0.217	41.6 ± 2.3	43.4 ± 2.6	144 ± 47
29, 1	0.00555	0.00033	0.0348	0.0023	0.0455	0.0009	98.7	80.8	0.95	8.26	90.3	1820	20	0.512	35.7 ± 2.1	34.7 ± 2.2	Negative
31, 1	0.00559	0.00047	0.0357	0.0032	0.0462	0.0016	99.7	94.8	0.92	7.51	89.9	3110	34	0.471	36.0 ± 3.0	35.6 ± 3.1	9.8 ± 83.1
32, 1	0.00423	0.00029	0.0264	0.0022	0.0452	0.0025	98.8	82.2	0.75	7.68	952	1370	1.4	0.919	**27.2 ± 1.9**	26.4 ± 2.1	negative
33, 1	0.00599	0.00037	0.0390	0.0026	0.0473	0.0010	99.6	92.7	0.94	7.78	67.4	2250	33	3.3	38.5 ± 2.4	38.9 ± 2.5	63.6 ± 51.8
34, 1	0.00400	0.00022	0.0247	0.0015	0.0449	0.0013	99.8	97.0	0.87	8.10	1279	1010	0.8	0.427	**25.7 ± 1.4**	24.8 ± 1.5	Negative
35, 1	0.00601	0.00044	0.0418	0.0337	0.0504	0.0392	78.4	17.6	0.44	8.18	92.5	2580	27	13.4	38.7 ± 2.8	41.6 ± 32.8	215 ± 1800
37, 1	0.00539	0.00050	0.0348	0.0035	0.0469	0.0014	99.9	97.4	0.96	7.43	67.6	1850	27	0.281	34.7 ± 3.2	34.8 ± 3.4	41.5 ± 69.7
43, 1	0.00682	0.00047	0.0440	0.0031	0.0468	0.0011	99.8	97.2	0.94	7.80	91.9	2480	26	0.0963	43.8 ± 3.0	43.7 ± 3.0	36.5 ± 57.4
43, 2	0.00736	0.00115	0.0476	0.0079	0.0469	0.0013	98.7	80.7	0.99	7.35	80.0	3480	42	4.75	47.3 ± 7.4	47.3 ± 7.7	45.2 ± 65.4
46, 1	0.00611	0.00037	0.0412	0.0031	0.0489	0.0016	99.8	96.9	0.90	8.07	123	1530	12	0.257	39.3 ± 2.4	41.0 ± 3.0	142 ± 76
47, 1	0.00311	0.00015	0.0190	0.0015	0.0443	0.0028	99.3	88.7	0.61	8.37	666	400	0.6	0.880	**20.0 ± 0.9**	19.1 ± 1.5	Negative
47, 2	0.0104	0.0008	0.0743	0.0054	0.0517	0.0013	99.8	96.7	0.94	8.00	247	992	3.9	0.0944	66.8 ± 4.8	72.7 ± 5.1	274 ± 57
47, 3	0.00753	0.00085	0.0486	0.0060	0.0468	0.0017	98.7	80.6	0.96	7.26	63.0	3130	48	5.07	48.4 ± 5.5	48.2 ± 5.8	40.5 ± 84.9

External reproducibility (1 standard deviation) of $^{206}Pb/^{238}U$ age of AS3 standard zircon 1.2% (April 21, 2009; n = 11) and 2.8% (July 09, 2009; n = 11). UO/U of standards between 7.6 and 8.2.
Spot ID–grain #, spot # (c indicates core spot; otherwise: rim).
$^{206}Pb^*/^{238}U$ ages shown in bold are interpreted to represent crystallization of the leucogranite.

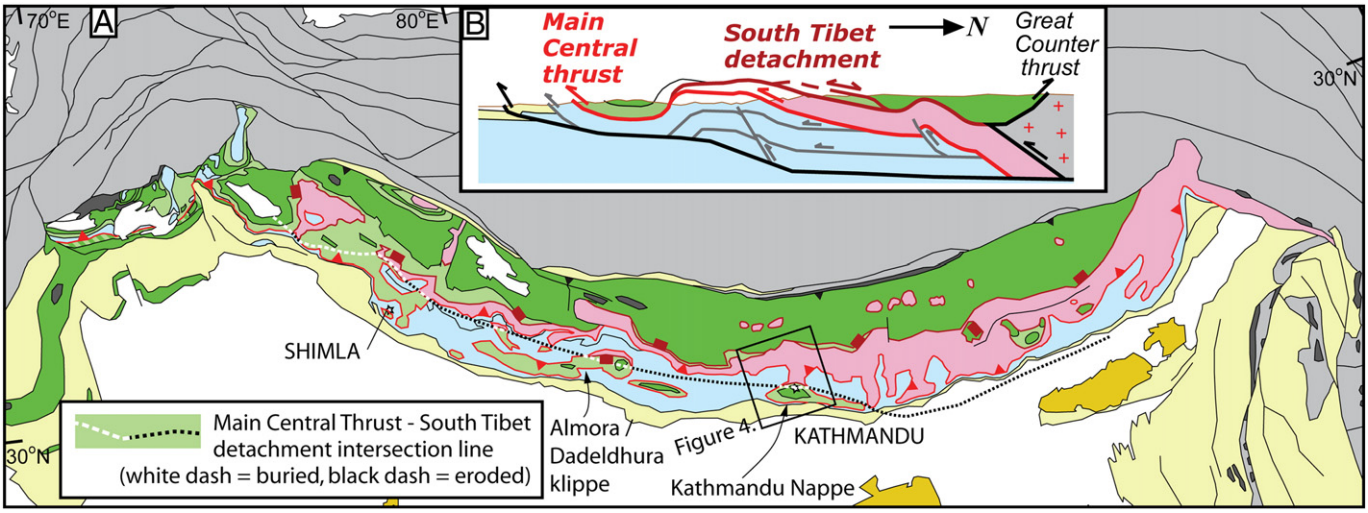

Fig. 9. A. Modified geological map of the Himalaya that incorporates a Main Central thrust–South Tibet detachment at the leading edge of the Greater Himalayan Crystalline Complex and shows rocks of the Bhimphedi Group as Tethyan Himalayan Sequence rocks to the south of the MCT–STD intersection line. Units as in Fig. 1. B. Schematic cross section across the central Himalaya.

They suggest that the fault may cut up-section to the south or expand and fade into a >10 km diffuse top-north deformation zone. However they focused their search for the South Tibet detachment by tracing a lithological contact that diverges from the metamorphic field gradient associated with this structure (described above). Therefore, it is possible that the basal South Tibet detachment shear zone persists further south. This latter interpretation is consistent with the southwards termination of the GHC proposed here.

5.2. Tectonic wedging kinematics across the Himalaya

The Himalayan architecture proposed here includes the local preservation of the leading edge of the GHC, and is therefore incompatible with wedge extrusion models and channel flow-focused denudation models which predict the extrusion of the GHC at the surface during the Early and Middle Miocene (Fig. 2). The only kinematic models that can accommodate this geometry are tectonic wedging models, although channel flow models in which tunneling persists throughout the Middle Miocene have essentially identical kinematics (as implied by Kellett and Godin, 2009, and Larson et al., 2010b). Surface processes and precipitation surely have a major role in shaping the entire orogenic evolution (e.g., Grujic et al., 2006; cf. Montgomery et al., 2001; Zeitler et al., 2001). However, given the tectonic architecture indicated by this work, the localized vertical uplift and exhumation due to focused erosion which is proposed as a major component of channel flow-focused exhumation models cannot have played a significant role in exhuming the GHC.

5.3. The thermal evolution of the South Tibet detachment

Tectonic wedging kinematics involves a reinterpretation of the South Tibet detachment. The fault was originally interpreted as a major normal fault (Burchfiel and Royden, 1985; Burg et al., 1984). Subsequent interpretations of the structure as a "back-stop fault" have maintained the footwall-up relative kinematics of normal faulting without involving net extension across the structure (e.g., Beaumont et al., 2001; Searle et al., 2003). Tectonic wedging, however, shows the South Tibet detachment as a north-directed thrust fault kinematically linked to the Great Counter thrust (Webb et al., 2007; Yin, 2006).

A north-directed thrust interpretation of the South Tibet detachment is relatively easy to envision in the context of lithologic juxtapositions. However the thermal pattern across the structure is a classic fit to a normal fault interpretation: colder rocks in the hanging wall, and hotter rocks in the footwall (e.g., Burchfiel et al., 1992; Burg et al., 1984). This pattern is not commonly associated with thrust faults. However, a comparison of tectonic wedging kinematics and channel tunneling kinematics shows that this thermal pattern could occur along a thrust. As noted above, these kinematic systems are remarkably similar: both involve top-north shearing along a sub-horizontal upper margin of the GHC (Fig. 2). The differences are timing of deformation phases, the presence of a top-south thrust fault extending southwards from the leading edge of the GHC, a top-north back thrust extending up from the South Tibet detachment, and alternating top-north and top-south shearing along the South Tibet detachment. However, some thermomechanical channel tunneling models do include these structures and alternating sense of shear, with top-north shear dominant (Beaumont et al., 2004).These show a clear northwards translation of colder rocks atop hotter rocks along the sub-horizontal South Tibet detachment (Beaumont et al., 2004). This comparison provides a basic understanding of how the South Tibet detachment can simultaneously accomplish shortening within the Himalaya and place colder rocks atop hotter rocks: subhorizontal shortening structures can juxtapose materials through dipping thermal gradients.

6. Conclusions

This contribution offers new structural and geochronological data along the Main Central thrust hanging wall transition from the Greater Himalayan Crystalline complex in the north to the enigmatic Bhimphedi Group in the south in the Kathmandu region. We identify an ~200 m thick top-north shear zone, the Galchi shear zone, occurring along the contact between these units at a site ~50 km west-northwest of Kathmandu. The shear zone appears to merge with the Main Central thrust to the south, bounding the leading edge of the Greater Himalayan Crystalline complex. On the bases of lithologic distribution, metamorphic field gradients, and shear kinematics, we interpret the Galchi shear zone as the southern extension of the South Tibet detachment and suggest that the southern Main Central thrust hanging wall is dominated by Tethyan Himalayan Sequence rocks. These interpretations, in combination with work in the western Himalaya (e.g., Thakur, 1998; Webb et al., 2007; Yin, 2006), indicate a Himalayan architecture in which the leading edge of the Greater Himalayan Crystalline complex is locally preserved along the length of the orogen. Wedge extrusion and channel flow-focused denudation models are precluded by this geometry, because they predict the surface emplacement of the Greater

Himalayan Crystalline complex in the Early–Middle Miocene and therefore require that the leading edge of the Greater Himalayan Crystalline complex has been eroded for ~15–20 Ma. Models that involve tectonic wedging kinematics, including channel tunneling models, can accomplish the proposed structural geometry and thermal evolution. The key structural geometry of a leading branch line of the Main Central thrust and South Tibet detachment has been determined by field mapping in only two locations, at this site and in the Shimla region (Fig. 1; Webb et al., 2007). Future work is required to evaluate its importance as an orogen-wide feature.

Acknowledgements

Suggestions of two anonymous reviewers and Editor Rick Carlson led to significant improvements in this work. We thank J.-P. Avouac, Julien Célérier, Peter DeCelles, Prashant Dubey, George Gehrels, Mark Harrison, Kyle Larson, Aaron Martin, Nadine McQuarrie, Michael Murphy, Randall Parrish, Lothar Ratschbacher, and An Yin for helpful discussions. Tracy Howe is gratefully acknowledged for support with geochronological analyses. We thank Bhim Chand and his colleagues at Earth's Paradise Treks and Adventures for field logistics. The ion microprobe facility at UCLA is partly supported by a grant from the Instrumentation and Facilities Program, Division of Earth Sciences, National Science Foundation. This research was supported by Fugro West, Inc and a start-up grant from Louisiana State University.

Appendix A. Supplementary data

Supplementary data to this article can be found online at doi:10.1016/j.epsl.2011.02.024.

References

Aikman, A.B., Harrison, T.M., Lin, D., 2008. Evidence for early (>44 Ma) Himalayan crustal thickening, Tethyan Himalaya, southeastern Tibet. EPSL 274, 14–23.
Argand, E., 1924. La Tectonique de l'Asie. Proc. Int. Geol. Cong. 7, 171–372.
Arita, K., Dallmeyer, R.D., Takasu, A., 1997. Tectonothermal evolution of the Lesser Himalaya, Nepal: constraints from Ar/Ar ages from the Kathmandu Nappe. Island Arc 6, 372–385.
Beaumont, C., Jamieson, R.A., Nguyen, M.H., Lee, B., 2001. Himalayan tectonics explained by extrusion of a low-viscosity crustal channel coupled to focused surface denudation. Nature 414, 738–742.
Beaumont, C., Jamieson, R.A., Nguyen, M.H., Medvedev, S., 2004. Crustal channel flows: 1. numerical models with applications to the tectonics of the Himalayan-Tibetan orogen. J. Geophys. Res. 109, B06406. doi:10.1029/2003JB002809.
Beyssac, O., Bollinger, L., Avouac, J.P., Goffe, B., 2004. Thermal metamorphism in the lesser Himalaya of Nepal determined from Raman spectroscopy of carbonaceous material. Earth Planet. Sci. Lett. 225, 233–241.
Bollinger, L., Janots, E., 2006. Evidence for Mio-Pliocene retrograde monazites from the lesser Himalayan metamorphic series in Far Western Nepal. Eur. J. Mineral. 18, 289–297.
Bollinger, L., Avouac, J.P., Beyssac, O., Catlos, E.J., Harrison, T.M., Grove, M., Goffé, B., Sapkota, S., 2004. Thermal structure and exhumation history of the Lesser Himalaya in central Nepal. Tectonics 23, TC5015. doi:10.1029/2003TC001564.
Bollinger, L., Henry, P., Avouac, J.P., 2006. Mountain building in the Nepal Himalaya: Thermal and kinematic model. Earth Planet. Sci. Lett. 244, 58–71.
Brown, R.L., Nazarchuk, J.H., 1993. Annapurna detachment fault in the Greater Himalaya of central Nepal. In: Treloar, P.J., Searle, M.P. (Eds.), Himalayan Tectonics: Geological Society Special Publication, 74, pp. 461–473.
Burchfiel, B.C., Royden, L.H., 1985. North–south extension within the convergent Himalayan region. Geology 13, 679–682.
Burchfiel, B.C., Chen, Z., Hodges, K.V., Liu, Y., Royden, L.H., Deng, C., Xu, J., 1992. The South Tibet Detachment system, Himalayan orogen. Extension Contemporaneous with and Parallel to Shortening in a Collisional Mountain Belt: Geological Society of America Special Paper, 269, pp. 1–41.
Burg, J.P., Brunel, M., Gapais, D., Chen, G.M., Liu, G.H., 1984. Deformation of leucogranites of the crystalline main central sheet in southern Tibet (China). J. Struct. Geol. 6, 535–542.
Catlos, E.J., Harrison, T.M., Kohn, M.J., Grove, M., Ryerson, F.J., Manning, C.E., Upreti, B.N., 2001. Geochronologic and thermobarometric constraints on the evolution of the Main Central Thrust, central Nepal Himalaya. J. Geophys. Res. Solid Earth 106 (B8), 16177–16204.
Catlos, E.J., Harrison, T.M., Manning, C.E., Grove, M., Rai, S.M., Hubbard, M.S., Upreti, B.N., 2002. Records of the evolution of the Himalayan orogen from in situ Th–Pb ion microprobe dating of monazite: Eastern Nepal and western Garhwal. J. Asian Earth Sci. 20, 459–479.
Catlos, E.J., Dubey, C.S., Harrison, T.M., Edwards, M.A., 2004. Late Miocene Movement within the Himalayan Main Central Thrust Shear Zone, Sikkim, NE India. Journal of Metamorphic Geology 22, 207–220.
Célérier, J., Harrison, T.M., Beyssac, O., Herman, F., Dunlap, W.J., Webb, A.A.G., 2009a. The Kumaun and Garwhal Lesser Himalaya, India; part 2, thermal and deformation histories. Geol. Soc. Am. Bull. 121, 1281–1297.
Célérier, J., Harrison, T.M., Webb, A.A.G., Yin, A., 2009b. The Kumaun and Garwhal Lesser Himalaya, India; part 1, structure and stratigraphy. Geol. Soc. Am. Bull. 121, 1262–1280.
Chambers, J., Caddick, M., Argles, T., Horstwood, M., Sherlock, S., Harris, N., Parrish, R., Ahmad, T., 2009. Empirical constraints on extrusion mechanisms from the upper margin of an exhumed high-grade orogenic core, Sutlej valley, NW India. Tectonophysics 477, 77–92.
Clift, P.D., Hodges, K., Heslop, D., Hannigan, R., Hoang, L.V., Calves, G., 2008. Correlation of Himalayan exhumation rates and Asian monsoon intensity. Nat. Geosci. 875–880.
Cottle, J.M., Jessup, M.J., Newell, D.L., Searle, M.P., Law, R.D., Horstwood, M.S.A., 2007. Structural insights into the early stages of exhumation along an orogen-scale detachment: the South Tibetan Detachment System, Dzakaa Chu section, Eastern Himalaya. J. Struct. Geol. 29, 1781–1797.
Daniel, C.G., Hollister, L.S., Parrish, R.R., Grujic, D., 2003. Exhumation of the Main Central Thrust from lower crustal depths, eastern Bhutan Himalaya. J. Metamorph. Geol. 21, 317–334.
DeCelles, P.G., Robinson, D.M., Quade, J., Ojha, T.P., Garzione, C.N., Copeland, P., Upreti, B.N., 2001. Stratigraphy, structure, and tectonic evolution of the Himalayan fold–thrust belt in western Nepal. Tectonics 20, 487–509.
Dèzes, P.J., Vannay, J.C., Steck, A., Bussy, F., Cosca, M., 1999. Synorogenic extension: quantitative constraints on the age and displacement of the Zanskar shear zone (northwest Himalaya). Geol. Soc. Am. Bull. 111, 364–374.
DiPietro, J.A., Pogue, K.R., 2004. Tectonostratigraphic subdivisions of the Himalaya: a view from the west. Tectonics 23, TC5001.
Epard, J.L., Steck, A., Vannay, J.C., Hunziker, J., 1995. Tertiary Himalayan structures and metamorphism in the Kulu Valley (Mandi–Khoksar transect of the Western Himalaya)–Shikar–Beh–Nappe and Crystalline Nappe. Schweiz. Mineral. Petrogr. Mitt. 75, 59–84.
Gansser, A., 1964. The Geology of the Himalayas. Wiley Interscience, New York. 289 pp.
Gehrels, G.E., DeCelles, P.G., Martin, A., Ojha, T.P., Pinhassi, G., Upreti, B.N., 2003. Initiation of the Himalayan Orogen as an early Paleozoic thin-skinned thrust belt. GSA Today 13 (9), 4–9.
Gehrels, G.E., DeCelles, P.G., Ojha, T.P., Upreti, B.N., 2006a. Geologic and U–Th–Pb geochronologic evidence for early Paleozoic tectonism in the Kathmandu thrust sheet, central Nepal Himalaya. Geol. Soc. Am. Bull. 118, 185–198.
Gehrels, G.E., DeCelles, P.G., Ojha, T.P., Upreti, B.N., 2006b. Geologic and U–Pbgeochronologic evidence for early Paleozoic tectonism in the Dadeldhura thrust sheet, far-west Nepal Himalaya. J. Asian Earth Sci. 28, 385–408.
Gleeson, T.P., Godin, L., 2006. The Chako antiform: a folded segment of the Greater Himalayan sequence, Nar valley, Central Nepal Himalaya. J. Asian Earth Sci. 27, 717–734.
Godin, L., Brown, R.L., Hanmer, S., 1999. High strain zone in the hanging wall of the Annapurna detachment, central Nepal Himalaya. In: Macfarlane, A., Sorkhabi, R.B., Quade, J. (Eds.), Himalaya and Tibet: Mountain Roots to Mountain Tops, Boulder, Colorado: Geological Society of America Special Papers, 328, pp. 199–210.
Godin, L., Parrish, R.R., Brown, R.L., Hodges, K.V., 2001. Crustal thickening leading to exhumation of the Himalayan Metamorphic core of central Nepal: insight from U–Pb Geochronology and Ar-40/Ar-39 Thermochronology. Tectonics 20 (5), 729–747.
Godin, L., Grujic, D., Law, R.D., Searle, M.P., 2006a. Channel flow, extrusion and exhumation in continental collision zones: an introduction. In: Law, R.D., Searle, M.P., Godin, L. (Eds.), Channel Flow, Ductile Extrusion and Exhumation in Continental Collision Zones: Geological Society of London Special Publication, 268, pp. 1–23.
Godin, L., Gleeson, T., Searle, M.P., Ullrich, T.D., Parrish, R.R., 2006b. Locking of southward extrusion in favor of rapid crustal-scale buckling of the Greater Himalayan sequence, Nar valley, central Nepal. In: Law, R.D., Searle, M.P., Godin, L. (Eds.), Channel Flow, Ductile Extrusion and Exhumation in Continental Collision Zones: Geological Society of London Special Publication, 268, pp. 269–292.
Grujic, D., Casey, M., Davidson, C., Hollister, L.S., Kundig, R., Pavlis, T., Schmid, S., 1996. Ductile extrusion of the Higher Himalayan Crystalline in Bhutan: evidence from quartz micro-fabrics. Tectonophysics 260, 21–43.
Grujic, D., Hollister, L.S., Parrish, R.R., 2002. Himalayan metamorphic sequence as an orogenic channel: insight from Bhutan. Earth Planet. Sci. Lett. 198, 177–191.
Grujic, D., Coutand, I., Bookhagen, B., Bonnet, S., Blythe, A., Duncan, C., 2006. Climatic forcing of erosion, landscape and tectonics in the Bhutan Himalayas. Geology 34, 801–804.
Harrison, T.M., Ryerson, F.J., LeFort, P., Yin, A., Lovera, O.M., Catlos, E.J., 1997. A Late Miocene–Pliocene origin for the Central Himalayan inverted metamorphism. Earth Planet. Sci. Lett. 146, E1–E7.
Harrison, T.M., Grove, M., Lovera, O.M., Catlos, E.J., 1998. A model for the origin of Himalayan anatexis and inverted metamorphism. J. Geophys. Res. 103, 27017–27032.
Hayashi, D., Fujii, Y., Yoneshiro, T., Kizaki, K., 1984. Observations on the geology of the Karnali Region, West Nepal. J. Nepal Geol. Soc. 4, 29–40.
Heim, A., Gansser, A., 1939. Central Himalaya Geological Observations of the Swiss Expedition 1936. Gebrüder Fretz, Zurich. 246 pp.
Herman, F., Copeland, P., Avouac, J.-P., Bollinger, L., Maheo, G., Le Fort, P., Rai, S., Foster, D., Pecher, A., Stuwe, K., Henry, P., 2010. Exhumation, crustal deformation, and thermal structure of the Nepal Himalaya derived from the inversion of thermochronological and thermobarometric data and modeling of the topography. JGR 115. doi:10.1029/2008JB006126.

Herren, E., 1987. Zanskar Shear Zone–Northeast–Southwest Extension within the Higher Himalayas (Ladakh, India). Geology 15 (5), 409–413.
Hodges, K.V., 2000. Tectonics of the Himalaya and southern Tibet from two perspectives. Geol. Soc. Am. Bull. 112 (3), 324–350.
Hodges, K.V., Parrish, R.R., Housh, T.B., Lux, D.R., Burchfiel, B.C., Royden, L.H., Chen, Z., 1992. Simultaneous Miocene extension and shortening in the Himalayan orogen. Science 258 (5087), 1466–1470.
Hodges, K.V., Parrish, R.R., Searle, M.P., 1996. Tectonic evolution of the central Annapurna Range, Nepalese Himalayas. Tectonics 15 (6), 1264–1291.
Hodges, K.V., Hurtado Jr., J.M., Whipple, K.X., 2001. Southward extrusion of Tibetan crust and its effect on Himalayan tectonics. Tectonics 20, 799–809.
Hoskin, P.W.O., Black, L.P., 2000. Metamorphic zircon formation by solid-state recrystallization of protolith igneous zircon. J. Metamorph. Geol. 18, 423–439.
Hubbard, M.S., 1996. Ductile shear as a cause of inverted metamorphism: example from the Nepal Himalaya. J. Geol. 104, 493–499.
Hubbard, M.S., Harrison, T.M., 1989. 40Ar/39Ar age constraints on deformation and metamorphism in the MCT Zone and Tibetan Slab, eastern Nepal Himalaya. Tectonics 8, 865–880.
Jain, A.K., Manickavasagam, R.M., Singh, S., 1999. Collision tectonics in the NW Himalaya: deformation, metamorphism, emplacement of leucogranite along Beas–Parbati Valleys, Himachal Pradesh. Gondwana Res. Group Mem. 6, 3–37.
Jamieson, R.A., Beaumont, C., Medvedev, S., Nguyen, M.H., 2004. Crustal channel flows: 2. numerical models with implications for metamorphism in the Himalayan–Tibetan orogen. J. Geophys. Res. 109, B06406. doi:10.1029/2003JB002811.
Jessup, M.J., Cottle, J.M., Searle, M.P., Law, R.D., Tracy, R.J., Newell, D.L., Waters, D.J., 2008. P–T–t–D paths of the Everest Series schist, Nepal. J. Metamorph. Geol. 26, 717–739.
Johnson, M.R.W., 2005. Structural settings for the contrary metamorphic zonal sequences in the internal and external zones of the Himalaya. J. Asian Earth Sci. 25, 695–706.
Johnson, M.R.W., Oliver, G.J.H., Parrish, R.R., Johnson, S.P., 2001. Synthrusting metamorphism, cooling, and erosion of the Himalayan Kathmandu complex, Nepal. Tectonics 20, 394–415.
Kellett, D.A., Godin, L., 2009. Pre-Miocene deformation of the Himalayan superstructure, Hidden valley, central Nepal. J. Geol. Soc. 166, 261–275.
Kellett, D.A., Grujic, D., Erdmann, S., 2009. Miocene structural reorganization of the South Tibetan detachment, eastern Himalaya: implications for continental collision. Lithosphere 1 (5), 259–281.
Kohn, M.J., 2008. P–T–t data from central Nepal support critical taper andrepudiate large-scale channel flow of the Greater Himalayan sequence. Geol. Soc. Am. Bull. 120, 259–273.
Kohn, M.J., Catlos, E.J., Ryerson, F.J., Harrison, T.M., 2001. Pressure–temperature–time path discontinuity in the Main Central thrust zone, central Nepal. Geology 29, 571–574.
Kohn, M.J., Wieland, M.S., Parkinson, C.D., Upreti, B.N., 2004. Miocene faulting at plate tectonic velocity in the central Himalaya, Nepal. Earth Planet. Sci. Lett. 228, 299–310.
Larson, K.P., Godin, L., Davis, J.D., Davis, D.W., 2010a. Out-of-sequence deformation and expansion of the Himalayan orogenic wedge: insight from the Changgo culmination, south central Tibet. Tectonics 29, 1–30. doi:10.1029/2008TC002393.
Larson, K.P., Godin, L., Price, R.A., 2010b. Relationships between displacement and distortion in orogens: linking the Himalayan foreland and hinterland in central Nepal. Geol. Soc. Am. Bull. 122, 1116–1134.
Le Fort, P., 1975. Himalayas–collided range–present knowledge of continental arc. Am. J. Sci. A275, 1–44.
Long, S., McQuarrie, N., 2010. Placing limits on channel flow: insights from the Bhutan Himalaya. Earth Planet. Sci. Lett. 290, 375–390.
Metcalfe, R.P., 1993. Pressure, temperature and time constraints on metamorphism across the Main Central Thrust zone and High Himalayan Slab in the Garhwal Himalaya. In: Treloar, P.J., Searle, M.P. (Eds.), Himalayan Tectonics: Geological Society Special Publication, 74, pp. 485–509.
Mitchell, A.H.G., Htay, M.T., Htun, K.M., Win, M.N., Oo, T., Hlaing, T., 2007. Rock relationships in the Mogok metamorphic belt, Tatkon to Mandalay, central Myanmar. J. Asian Earth Sci. 29, 891–910.
Montgomery, D.R., Balco, G., Willett, S.D., 2001. Climate, tectonics, and the morphology of the Andes. Geology 29, 579–582.
Nelson, K.D., 1996. Partially molten middle crust beneath southern Tibet: synthesis of project INDEPTH results. Science 274, 1684–1688.
Paces, J.B., Miller, J.D., 1993. Precise U–Pb age of the Duluth Complex and related mafic intrusions, northeastern Minnesota: geochronological insights in physical, petrogenetic, paleomagnetic, and tectonomagmatic processes associated with the 1.1 Ga midcontinent rift system. J. Geophys. Res. 98, 13997–14013.
Patel, R.C., Singh, S., Asokan, A., Manickavasagam, R.M., Jain, A.K., 1993. Extensional tectonics in the Himalayan orogen, Zanskar, NW India. In: Treloar, P.J., Searle, M.P. (Eds.), Himalayan Tectonics: Geological Society Special Publication, 74, pp. 445–459.
Pearson, O.N., DeCelles, P.G., 2005. Structural geology and regional significance of the Ramgarh thrust, Himalayan fold–thrust belt of Nepal. Tectonics 24 (4), TC4008. doi:10.1029/2003TC001617.
Powell, C.McA., Conaghan, P.J., 1973. Plate tectonics and the Himalayas. Earth Planet. Sci. Lett. 20, 1–12.
Rai, S.M., Guillot, S., LeFort, P., Upreti, B.N., 1998. Pressure–temperature evolution in the Kathmandu and Gosainkund regions, Central Nepal. J. Asian Earth Sci. 16, 283–298.
Rao, V.V., Prasad, B.R., Reddy, P.R., Tewari, H.C., 2000. Evolution of Proterozoic Aravalli Delhi Fold Belt in the northwestern Indian Shield from seismic studies. Tectonophysics 327, 109–130.
Robinson, D.M., Pearson, O.N., 2006. Exhumation of Greater Himalayan rock along the Main Central Thrust in Nepal; implications for channel flow. In: Law, R.D., Searle, M.P., Godin, L. (Eds.), Channel Flow, Ductile Extrusion and Exhumation in Continental Collision Zones: Geological Society of London Special Publication, 268, pp. 255–267.
Robinson, D.M., DeCelles, P.G., Garzione, C.N., Pearson, O.N., Harrison, T.M., Catlos, E.J., 2003. Kinematic model for the Main Central Thrust in Nepal. Geology 31, 359–362.
Robinson, D.M., DeCelles, P.G., Copeland, P., 2006. Tectonic evolution of the Himalayan thrust belt in western Nepal: implications for channel flow models. Geol. Soc. Am. Bull. 118, 865–885.
Rubatto, D., 2002. Zircon trace element geochemistry: partitioning with garnet and the link between U–Pb ages and metamorphism. Chem. Geol. 184, 123–138.
Rubatto, D., Hermann, J., Buick, I.S., 2006. Temperature and bulk composition control on the growth of monazite and zircon during low-pressure anatexis (Mount Stafford, Central Australia). J. Petrol. 47 (10), 1973–1996.
Schelling, D., Arita, K., 1991. Thrust tectonics, crustal shortening, and the structure of the far-eastern Nepal Himalaya. Tectonics 10, 851–862.
Schmitt, A.K., Grove, M., Harrison, T.M., Lovera, O.M., Hulen, J., Walters, M., 2003. The Geysers - Cobb Mountain Magma System, California (Part 1): U-Pb zircon ages of volcanic rocks, conditions of zircon crystallization and magma residence times. Geochim. Cosmochim. Acta 67 (18), 3423–3442.
Searle, M.P., 1986. Structural evolution and sequence of thrusting in the High Himalayan, Tibetan-Tethys and Indus suture zones of Zanskar and Ladakh, Western Himalaya. Journal of Structural Geology 8 (8), 923–936.
Searle, M.P., Godin, L., 2003. The South Tibet Detachment and the Manaslu Leucogranite: a structural re-interpretation and restoration of the Annapurna–Manaslu Himalaya, Nepal. J. Geol. 111, 505–523.
Searle, M.P., Parrish, R.R., Hodges, K.V., Hurford, A., Ayres, M.W., Whitehouse, M.J., 1997. Shisha Pangma leucogranite, South Tibetan Himalaya: field relations, geochemistry, age, origin and emplacement. J. Geol. 105, 295–317.
Searle, M.P., Simpson, R.L., Law, R.D., Parrish, R.R., Waters, D.J., 2003. The structural geometry, metamorphic and magmatic evolution of the Everest massif, High Himalaya of Nepal–south Tibet. J. Geol. Soc. Lond. 160, 345–366.
Searle, M.P., Law, R.D., Godin, L., Larson, K.P., Streule, M.J., Cottle, J.M., Jessup, M.J., 2008. Defining the Himalayan Main Central Thrust in Nepal. J. Geol. Soc. 164, 523–534.
Stacey, J.S., Kramers, J.D., 1975. Approximation of terrestrial lead isotope evolution by a two-stage model. Earth Planet. Sci. Lett. 26, 207–221.
Stöcklin, J., 1980. Geology of Nepal and its regional frame. J. Geol. Soc. 137, 1–34.
Stöcklin, J., and Bhattarai, K.D., 1982, Photogeological map of part of central Nepal: Kathmandu, Ministry of Industry and Commerce, Department of Mines and Geology, scale 1:100, 000.
Thakur, V.C., 1998. Structure of the Chambanappew and position of the main central thrust in Kashmir Himalaya. J. Asian Earth Sci. 16, 269–282.
Thiede, R.C., Bookhagen, B., Arrowsmith, J.R., Sobel, E.R., Strecker, M.R., 2004. Climatic control on rapid exhumation along the Southern Himalayan Front. Earth Planet. Sci. Lett. 222 (3–4), 791–806.
Thiede, R.C., Arrowsmith, J.R., Bookhagen, B., McWilliams, M.O., Sobel, E.R., Strecker, M.R., 2005. From tectonically to erosionally controlled development of the Himalayan fold-and-thrust belt. Geology 33, 689–692.
Upreti, B.N., Le Fort, P., 1999. Lesser Himalayan crystalline nappes of Nepal: problems of their origin. Geological Society of America Special Paper, 328, pp. 225–238.
Valdiya, K.S., 1980. Geology of Kumaun Lesser Himalaya. Wadia Institute of Himalayan Geology, Dehra Dun, India. 291 pp.
Valdiya, K.S., 1989. Trans-Himadri intracrustal fault and basement up warps south of Indus–Tsangpo Suture Zone. GSA Special Paper, 232, pp. 153–168.
Vannay, J.C., Grasemann, B., 1998. Inverted metamorphism in the High Himalaya of Himachal Pradesh (NW India): phase equilibria versus thermobarometry. Schweiz. Mineral. Petrogr. Mitt. 78, 107–132.
Vannay, J.C., Sharp, Z.D., Grasemann, B., 1999. Himalayan inverted metamorphism constrained by oxygen isotope thermometry. Contrib. Mineralog. Petrol. 137 (1–2), 90–101.
Vannay, J.C., Grasemann, B., Rahn, M., Frank, W., Carter, A., Baudraz, V., Cosca, M., 2004. Miocene to Holocene exhumation of metamorphic crustal wedges in the NW Himalaya: evidence for tectonic extrusion coupled to fluvial erosion. Tectonics 23, TC1014.
Webb, A.A.G., Yin, A., Harrison, T.M., Célérier, J., Burgess, W.P., 2007. The leading edge of the Greater Himalayan Crystallines revealed in the NW Indian Himalaya: implications for the evolution of the Himalayan Orogen. Geology 35, 955–958.
Wiedenbeck, M., Alle, P., Corfu, F., Griffin, W.L., Meier, M., Oberli, F., von Quadt, A., Roddick, J.C., Spiegel, W., 1995. Three natural zircon standards for U–Th–Pb, Lu–Hf, trace element and REE analyses. Geostand. Newsl. 19, 1–23.
Wobus, C.W., Heimsath, A.M., Whipple, K.X., Hodges, K.V., 2005. Active out-of-sequence thrust faulting in the central Nepalese Himalaya. Nature 434, 1008–1011.
Yin, A., 2006. Cenozoic tectonic evolution of the Himalayan orogen as constrained by along-strike variation of structural geometry, exhumation history, and foreland sedimentation. Earth Sci. Rev. 76, 1–131.
Yin, A., Harrison, T.M., 2000. Geologic evolution of the Himalayan-Tibetan orogen. Annu. Rev. Earth Planet. Sci. 28, 211–280.
Yin, A., Harrison, T.M., Ryerson, F.J., Chen, W., Kidd, W.S.F., Copeland, P., 1994. Tertiary structural evolution of the Gangdese thrust system, southeastern Tibet. J. Geophys. Res. 99, 18175–18201.
Yin, A., Harrison, T.M., Murphy, M.A., Grove, M., Nie, S., Ryerson, F.J., Wang, X.F., Chen, Z.L., 1999. Tertiary deformation history of southeastern and southwestern Tibet during the Indo-Asian collision. GSA Bull. 111 (11), 1644–1664.
Yin, A., Dubey, C.S., Kelty, T.K., Webb, A.A.G., Harrison, T.M., Chou, C.Y., Celerier, J., 2010. Geologic correlation of the Himalayan orogen and Indian craton: part 2. Structural geology, geochronology, and tectonic evolution of the Eastern Himalaya. GSA Bull. 122, 360–395.
Zeitler, P.K., Meltzer, A.S., Koons, P.O., Craw, D., Hallet, B., Chamberlain, C.P., Kidd, W.S.F., Park, S.K., Seeber, L., Bishop, M., Shroder, J., 2001. Erosion, Himalayan geodynamics, and the geomorphology of metamorphism. GSA Today 11, 4–9.